

# AIRCRAFT NOISE SIMULATION ENVIRONMENT, SUITABLE FOR DEVELOPMENT OF NOISE ABATEMENT PROCEDURES

**Anton C. de Bruin, Marthijn Tuinstra**  
National Aerospace Laboratory NLR

**Keywords:** *Flight simulation; Engine simulation; Noise prediction*

## Abstract

*Noise production in the vicinity of (military) airports is of continued concern, especially for aircraft during the (high thrust) take-off phase. Many airports are operated under law enforced noise contour limitations. In an attempt to cope with this, noise abatement flight procedures are being considered.*

*A noise prediction environment is presented that combines the simulation of aircraft trajectory, attitude, speed and thrust with a simulation of the corresponding noise characteristics of the engine. The method couples a flight simulation method with the NLR Gas Turbine Simulation Program (GSP) and a noise prediction model.*

*In the present paper the developed simulation tool has been applied to several flight conditions of the F-16 fighter. Straight and turning level flights and parametric take-off simulations are being considered. It is shown that significant noise reductions can be obtained in the climb-out region around the airport by adapted take-off procedures.*

## 1 Introduction

A combined flight mechanics, gas turbine simulation and noise prediction tool (E-NoiSE Engine Noise Simulation Environment) has been developed. The three elements of this tool are displayed in Figure 1. The current tool takes into account jet mixing noise only. This is seen as a first step, since the method can be extended with fan-noise and airframe-noise prediction models, which will certainly be needed for civil aircraft noise predictions. In the present paper the tool has been applied to a military fighter

aircraft case, for which jet mixing noise is considered to be the major noise source. A brief description of the simulation method is given in the next subsections.

### 1.1 Flight simulation method

For the present application a Matlab-Simulink based flight simulation model (see [1], [3]) for the prediction of aircraft trajectory, aircraft attitude and required thrust (or throttle setting) is used. It contains a 6-Degree Of Freedom (6-DOF) flight mechanics model for the F-16 aircraft. Force and moment coefficients are prescribed by tabulated data. E.g. lift and drag coefficients are tabulated as function of Mach number, angle of attack and side slip and as function of control surface deflections (rudder, aileron, trailing edge and leading edge flaps). Either a low or a high fidelity representation of the aerodynamic coefficients can be used. The low fidelity model [1] uses a simplified aerodynamic model, in which the effect of the leading edge flap (LEF) is implicitly taken into account. In the more accurate high fidelity model [2], used in the present study, the LEF deflection is explicitly taken into account. The leading edge flap deflection is automatically controlled depending on angle of attack  $\alpha$  and Mach number. The LEF improves the lift over drag ratio at high angles of attack. In the present study mainly symmetric flight conditions are considered, for which the flight mechanics model is effectively reduced to a 3-DOF model.

The original flight mechanics model was augmented with a flap extension model, necessary to simulate take-off's, and adapted to enable simulations for non-ISA atmospheric conditions (including headwinds). Dedicated

auto-pilot models were developed for the acceleration phase on the ground, the initial climb phase at constant pitch angle  $\theta$  and the continued climb at constant calibrated airspeed (KCAS). Figure 2 shows, as an example, the Pitch Attitude Hold (PAH) auto-pilot model for the second climb segment at a given throttle setting. The parameterized take-off flight scenario is controlled by user input. In the simulations throttle setting  $th$  is used to control the engine. In the present simulations the engine throttle setting  $th$  was less than 0.74, so below the military power throttle setting of 0.77. Note that full After Burner (AB) power setting corresponds to a throttle setting of 1.00.

An output file is produced that contains for each time step a line with the following data: time ( $t$ ), aircraft positions ( $x, y, z$ ), airspeed ( $V_t$ ), roll, pitch and yaw angle ( $\phi, \theta, \psi$ ), angle of attack and side-slip ( $\alpha, \beta$ ), angular velocities ( $p, q, r$ ) and the engine thrust force ( $F_T$ ). For non-ISA conditions static pressure ( $p$ ) and static temperature ( $T$ ) are also added. Horizontal headwind  $V_H$  can also be taken into account. In this paper all calculations were made for a typical training configuration of the F-16 fighter aircraft ( $m=11190$  kg) and zero wind ISA (International Standard Atmosphere) atmospheric conditions, unless stated otherwise.

### 1.2 Engine simulation model

For the analysis of (off-line) propulsion system performance, NLR has developed the Gas turbine Simulation Program (GSP, see [6]). This tool is capable of calculating both steady-state and transient gas turbine performance using a user-friendly drag & drop interface with on-line help running under MS-Windows. GSP has a modular set-up, each engine component is primarily based on OD-modelling of the flow properties, averaged over the flow cross section areas at the interface surfaces of the component models (inlet and exit). GSP utilizes component model stacking to create the thermodynamic cycle of the engine of interest. The exit gas condition of a component forms the inlet gas condition for the next component in the configuration. Processes in gas turbine components are determined by relations among

2 up to 5 parameters defined by component maps and thermodynamic equations. These parameters are air or gas properties and other parameters such as rotor speeds and efficiencies determining the component operating point. Here an existing and well validated model for the double spool F100-PW-220 turbofan engine of the F-16 is used. The GSP modular model is shown in Figure 3. Engine properties are computed at a given thrust  $F_T$  or power setting (Power Lever Angle, PLA).

In the current application the output file from the flight simulation is used as input to GSP in order to compute the physical properties of the engine exhaust jet (velocity, temperature, Mach number and cross sectional area of the jet), for given thrust force  $F_T$ , at discrete points along the flight track.

### 1.3 Noise prediction model

The combined results of the flight simulation and GSP method provide the necessary inputs for the noise computation. The noise modeling has been integrated into GSP environment (see figure 3). The emitted jet mixing noise is computed with the updated version [4] of the method that was originally developed by Stone and Montegani [5]. It takes account of the aircraft velocity, jet velocity, jet Mach number, jet cross sectional area, the distance between the observer and the noise source, the angle between the jet axis and the position vector to the observer and the movement of the noise-source with respect to the observer. Atmospheric attenuation [7], acoustic reflections with the ground [8] and [9] and impedance modeling [10] are also taken into account.

For each time-step the computed instantaneous noise levels are stored on a user-defined grid below the flight path, here taken at 1.2 m above the ground. From these data various results can be computed, e.g.  $L_{A,max}$  or  $L_{A,den}$ . Also noise spectra can be computed at dedicated (or all) grid points.

In this paper results are presented, either as A-weighted Overall Sound Pressure Level (OASPL)  $L_A$  at a certain noise emission time, or as  $L_{A,max}$  noise levels.

## 2 Application to level flights

Steady level flights, either straight or turning, pose a significant part of normal day-to-day operations. Noise contours will depend on the flight altitude and on aircraft speed, because aircraft speed defines the required thrust and aircraft pitch angle. Trimmed steady level straight and turning flight conditions were simulated, using dedicated trim routines, in order to show the effect of aircraft speed on noise contours. Trailing edge flaps and undercarriage were retracted during these flight simulations.

### 2.1 Straight level flights

As an example, trimmed straight steady level flight conditions were computed at an altitude of 1500 m for true aircraft speeds  $V_t$  between 70 and 250 m/s. For horizontal flight, the pitch angle is equal to the angle of attack and depends on the flight speed, as shown in Figure 4. The lift and drag coefficients depend on angle of attack  $\alpha$ . As shown in Figure 5, the maximum lift to drag ratio is obtained near  $\alpha = 4$  deg, which, at an altitude of 1500 m and for the chosen aircraft mass of 11190 kg, corresponds to a true airspeed  $V_t$  of about 150 m/s (see figure 4). At this speed the required thrust for straight level flight attains its minimum value, as shown in figure 6. Note that at low speed, because of the high pitch angle, a significant part of the vertical force that balances the weight comes from the engine thrust. Leading edge flap and required elevator deflections are shown in Figure 7 and Figure 8. At high angle of attack (low speeds) the leading edge flap is deflected up to its maximum value of 25 deg and the elevator needs to be deflected upwards to about 6 deg for maintaining zero pitching moment for stationary horizontal flight.

Because of the jet noise directivity, the pitch angle has a (minor) effect on the computed noise contour. A comparison of instantaneous noise footprints,  $L_A$ , for aircraft flying in  $x$  direction at true airspeeds  $V_t$  of 250, 200, 150 or 100 m/s, is given in Figure 9. The position of

the aircraft at the time of the instantaneous noise contour is indicated with a blue dot. Only half of the symmetric noise footprint is shown. The jet noise directivity is clearly visible in these figures. Corresponding to the thrust demand at the different speeds, shown in figure 6, relatively high noise levels are found both for the low and high speed case. The lowest noise levels are obtained for the  $V_t = 150$  m/s case, a condition close to  $C_L/C_{D,max}$  and thus near minimum thrust.  $L_{A,max}$  values for the different aircraft speeds are shown as function of the lateral distance to the flight path in Figure 10. Depending on aircraft speed, differences up to 10 dBA are observed.

### 2.2 Level coordinated turns

As an example, steady level coordinated turning flights (meaning zero lateral acceleration in the aircraft coordinate system) with a centripetal acceleration  $a_c$  of 1g (9.8065 m/s<sup>2</sup>) are considered here. These correspond with an aircraft bank angle of about 45 deg. The turn radius is proportional to  $V_t^2$ . For  $a_c = 1$  the turn radius becomes 500 m at  $V_t = 70$  m/s and 6373 m at  $V_t = 250$  m/s. For a given airspeed, steady level turns require a larger lift, and thus a larger angle of attack (see Figure 4), than straight level flights. The higher lift leads to a higher drag value and a higher thrust demand (see Figure 6). The leading edge flap and elevator deflections are shown as function of angle of attack in Figure 7 and Figure 8. The leading edge flap angle is also a function of Mach number  $Ma$ . For a given value of  $\alpha$ , the Mach numbers for straight and turning flight are different, leading to a small difference in leading edge flap angle.

The computed  $L_{A,max}$  noise contour for a complete steady level turn (colored levels) and instantaneous noise contours (black lines) for the aircraft at the blue dot position, flying in a counter clockwise direction along the circular trajectory (indicated by the white line) with  $a_c = 1$  and  $V_t = 250$  m/s, are shown in Figure 11. A comparison of  $L_{A,max}$  values at different aircraft speeds is shown as function of the radial distance to the turn centre point in Figure 12. At low speed the turn requires high thrust, leading to a higher noise level.

### 3 Application to take-off's

Relatively high thrust levels are needed during take-off in order to accelerate the aircraft on the runway and safely climb thereafter. Take-offs contribute significantly to the total noise produced around military airfields. Normally the initial take-off phase is made at a constant high throttle setting (either at military or full AB power) and after rotation and take-off the flight is continued at a fixed constant pitch angle. When reaching a certain airspeed and/or altitude it is possible to continue the climb with a different climb strategy, e.g. by applying a power cutback or switching to a steeper approach at constant *KCAS*. In a first study, parametric take-off simulations were made and resulting take off trajectories and noise footprints have been compared in order to devise noise abatement take off procedures.

#### 3.1 The take-off simulation model

For the parametric study of take-off's, the aircraft trajectory is build up by a series of piecewise continuous simulations, allowing discontinuous changes of some of the parameters in between these phases. It is organized as follows:

- 1) User input of take-off simulation parameters: initial altitude; final altitude for level flight; initial throttle setting; final throttle setting after reaching *KCAS*; pitch angle  $\theta$  during initial take-off; *KCAS* for the final climb segment and the maximum simulation time.
- 2) Determination of lift-off velocity  $V_{LOF}$  at user prescribed pitch angle  $\theta$ , for aircraft with flaps deflected.
- 3) Ground acceleration phase at  $\alpha = \theta = 0$  until reaching rotation speed  $V_r = 0.89V_{LOF}$  (from empirical fit). The friction with the ground is taken into account.
- 4) Change to prescribed pitch angle  $\theta$  and continue the ground acceleration until reaching  $V_{LOF}$ .
- 5) Initial climb with Pitch Attitude Hold (PAH) auto-pilot model. If the difference between  $\theta$  and  $\alpha$  becomes more than 2 deg ( $\alpha$  decreases

because of aircraft acceleration), the flaps and undercarriage are retracted and the PAH simulation is continued until *KCAS* is reached.

6) Now throttle setting is adapted to the user prescribed value for the 2<sup>nd</sup> climb segment and the aircraft pitch angle is changed to a trimmed condition for climb at constant *KCAS*. The simulation is continued with auto pilot model CASH for constant *KCAS* until final altitude is reached.

7) At the final altitude the aircraft is re-trimmed for steady level flight with reduced throttle setting.

#### 3.2 Take-off simulation results

All take-off simulations were made with the pitch angle for the PAH simulation on the first climb segment set at 10 deg, the initial throttle setting was just below that of military power ( $th = 0.74$  instead of 0.77) and a final altitude of 1500 m was prescribed. Position  $x = 0$  is at the start of the ground acceleration phase. Three sets of calculations were made.

In the first set of calculations *KCAS* on the second climb segment was varied (250, 300 and 350 *KCAS*). Figure 13 shows the aircraft trajectories. When *KCAS* is low the (steeper) 2<sup>nd</sup> climb segment starts earlier. Pitch angle and angle of attack are shown as function of distance  $x$  in Figure 14 and 15. Note that, with the present aircraft weight, at *KCAS* = 250 the angle of attack is close to 4 deg, the condition for minimum drag which provides maximum climb for a given throttle setting. Figure 16 shows the thrust as function of distance  $x$ . The effect of the thrust cutback when reaching final altitude, is clearly visible in the noise footprints for  $L_{A,max}$  that are shown in figure 17.

A second set of calculations was made for *KCAS* = 250, but now with reduced throttle settings on the 2<sup>nd</sup> climb segment ( $th = 0.40, 0.60$  and  $0.74$ ). Figure 18 shows the aircraft trajectories, figure 19 the pitch angle and figure 20 the engine thrust. Figure 21 shows the corresponding  $L_{A,max}$  noise footprints. Power cut-back leads to a reduced climb rate, but less thrust and therefore less produced noise during the 2<sup>nd</sup> climb phase. For a further explanation of the results, figure 22 shows the aircraft

trajectories for the  $th= 0.74$  and  $th= 0.40$  cases, together with predicted  $L_{A,max}$  values at position  $y= 1000$  m aside from the flight track. For the case without power cutback the noise results of the different flight phases are shown separately. The red line shows  $L_{A,max}$  for the ground acceleration and initial climb phase. Due to sound directivity the maximum jet noise is radiated at about 135 deg from the flight direction. With the aircraft still at low altitude, at  $y= 1000$  m aside from the track, the maximum noise will thus be found at about 1000m aft of the aircraft. Indeed the maximum noise level is observed at about 1300 m and not at the end of the 1<sup>st</sup> climb segment ( $x= 2300$  m). The solid blue line shows  $L_{A,max}$  until reaching the final altitude. For low  $x$  values, the noise produced on the 2<sup>nd</sup> climb segment apparently dominates over the noise produced over the initial climb phase. This can be understood, because during the continued climb the angle between the radiated noise and the ground increases, which leads to reduced noise absorption at the ground. The very low noise produced during the level flight segment at 1500 m altitude is indicated by the magenta line and it only starts to dominate  $L_{A,max}$  beyond  $x= 11000$  m.

For the case with power cutback only the noise produced during the 2<sup>nd</sup> climb phase is shown (broken blue line). Due to the power cutback a stepwise change in produced noise occurs. Total  $L_{A,max}$  then follows as the max value from the 1<sup>st</sup> and 2<sup>nd</sup> climb segment (the red line at low and the broken blue line at large values of  $x$ ). These observations do well explain the shape of the noise contours that were shown in figure 21.

Finally, additional simulations were made for a take-off scenario with  $KCAS=300$  on the 2<sup>nd</sup> climb segment, without and with a quite strong headwind of 15 m/s at 10 m height. A simple power law scaling of headwind with altitude was used in this example. Figure 23 compares the aircraft trajectory with- and without headwind and figure 24 compares the noise footprints. The main effect is that, with headwind, the final altitude and related power cut-back is reached at a lower  $x$  value, leading to a somewhat “shorter” noise contour.

#### 4 Concluding remarks

A simulation environment for predicting noise contours, E-NoiSE, was developed. It combines flight mechanics, engine performance and noise prediction in a closely coupled simulation tool. At present, only jet mixing noise is taken into account, but this will be extended with shock noise, fan noise and possibly also airframe noise modules. Validation of the method against flyover noise tests is in progress. With all prime parameters taken into account the tool can be used both for simulation of daily operations as well as for studying noise abatement procedures.

The method is demonstrated for straight and turning level flights and with some parametric take-off simulations for a fighter aircraft.

The same modeling strategy can also be applied to civil aircraft operations, provided a tailored flight mechanics and GSP engine model is available. Instead of MATLAB-Simulink flight simulation results, it is possible to use alternative input sources for the engine and noise simulation with GSP. E.g. results from piloted flight simulations or actual measured flight data.

#### References

- [1] Stevens B.L., Lewis F.L.: *Aircraft control and simulation*, John Wiley & Sons, Inc., 1992.
- [2] Nguyen L.T., Ogburn M.E., Gilbert W.P., Kibler K.S., Brown Ph. W., Deal P.L.: *Simulator study of stall/post-stall characteristics of a fighter airplane with relaxed longitudinal static stability*, NASA TP 1538.
- [3] Sonneveldt L.: *Nonlinear F-16 model description*, version 0.3, June 2009.
- [4] Stone J.R., Zola C.L., Clark B.J.: *An improved prediction method for conventional and inverted velocity-profile co-annular jet noise*, AIAA-99-0078.
- [5] Stone J.R., Montegani F.J.: *An improved prediction method for the noise generated in flight by circular jets*, NASA TM 81470, 1980.
- [6] Visser W.P.J., Broomhead M.J.: *GSP A generic object-oriented gas turbine simulation environment*, NLR-TP-2000-267.
- [7] Bass H.E., Zuckerwar L.C., Blackstock D.T., Sutherland L.C.: *Atmospheric absorption of sound: further developments*, Journal of Acoustic Society of America, 97, pp. 680-683, 1995.



**AN AIRCRAFT NOISE SIMULATION ENVIRONMENT, SUITABLE FOR THE DEVELOPMENT OF NOISE ABATEMENT PROCEDURES**

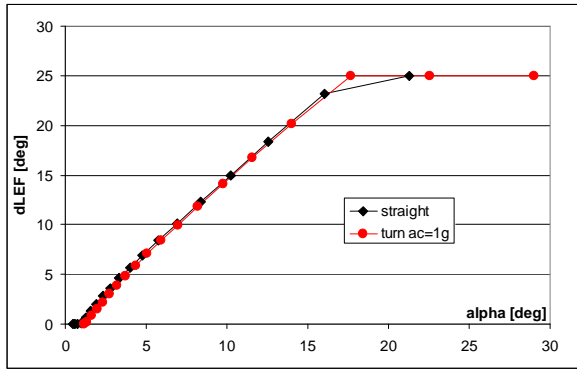


Figure 7: Leading edge flap deflection angle as function of angle of attack (different  $V_t$ ), for steady straight and turning level flights with an F-16 aircraft at  $a_c = 1g$ ,  $h = 1500$  m.

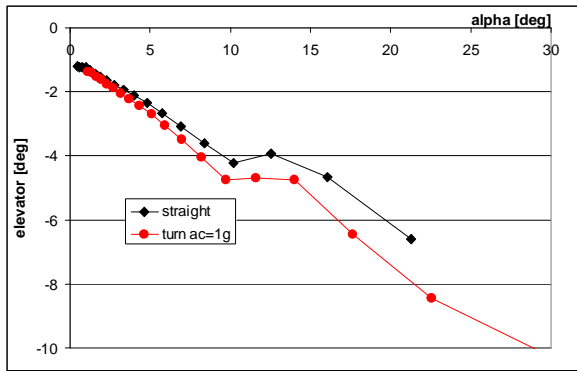


Figure 8: Elevator deflection angle as function of angle of attack (different velocities), for steady straight and turning level flights with an F-16 aircraft at  $a_c = 1g$ ,  $h = 1500$  m.

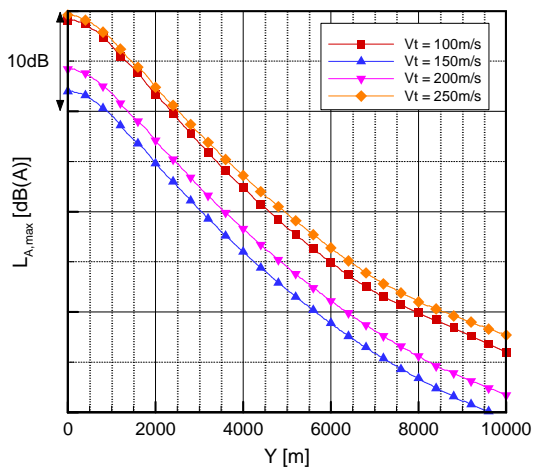
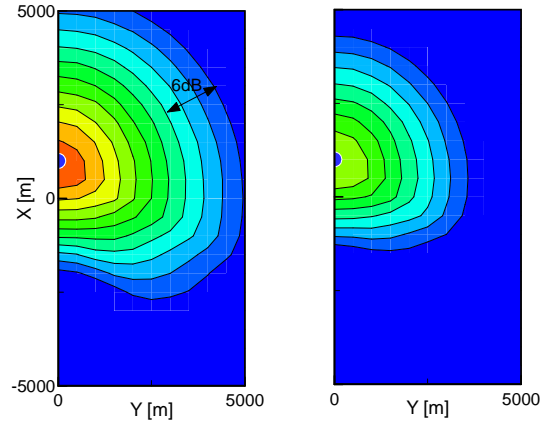
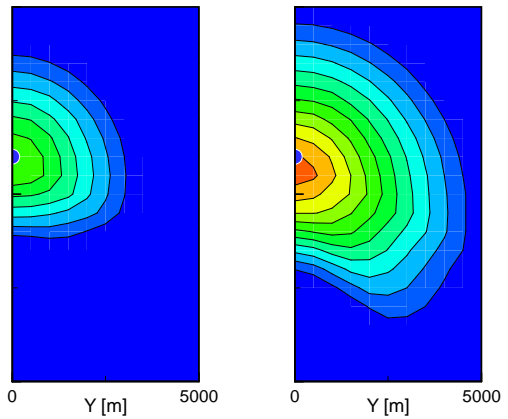


Figure 9:  $L_{A,max}$  as function of lateral distance to flight path, steady straight level flights with an F-16 aircraft at  $h = 1500$  m at various speeds  $V_t$ .



a)  $V_t = 250$  m/s

b)  $V_t = 200$  m/s



c)  $V_t = 150$  m/s

d)  $V_t = 100$  m/s

Figure 10: Comparison of instantaneous noise footprints  $L_A$  for horizontal flights with an F-16 aircraft at  $h = 1500$  m, different airspeeds  $V_t$ . The aircraft is at  $X = 1000$  m (indicated by the blue dot).

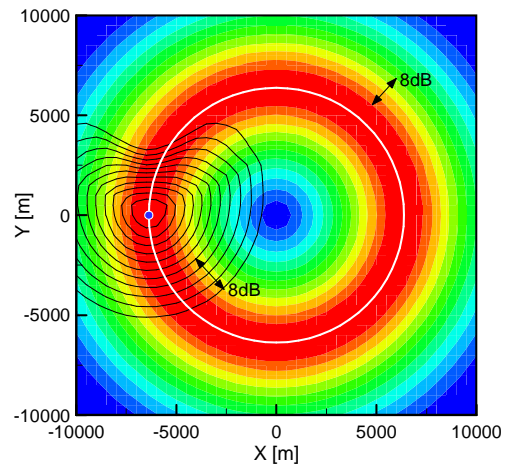


Figure 11: Noise footprint  $L_{A,max}$  (colored levels) and an instantaneous noise footprint  $L_A$  (black lines, for aircraft at blue dot position,  $Y = 0$ ) for a steady level turn with an F-16 aircraft at  $a_c = 1g$  and  $V_t = 250$  m/s.

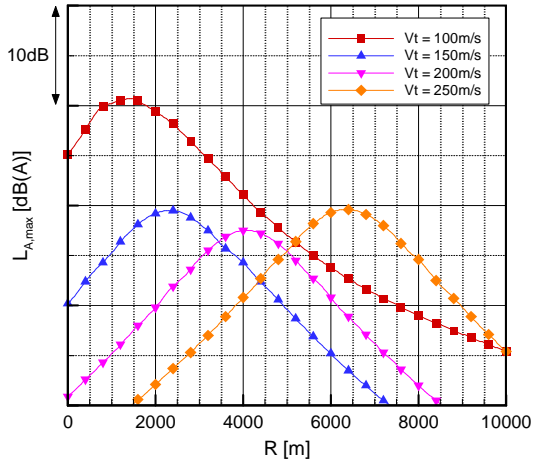


Figure 12:  $L_{A,max}$  as function of the radial distance to the flight path, steady level turns with an F-16 aircraft at  $\alpha_c = 1g$ ,  $h = 1500$  m and for different values of  $V_t$ .

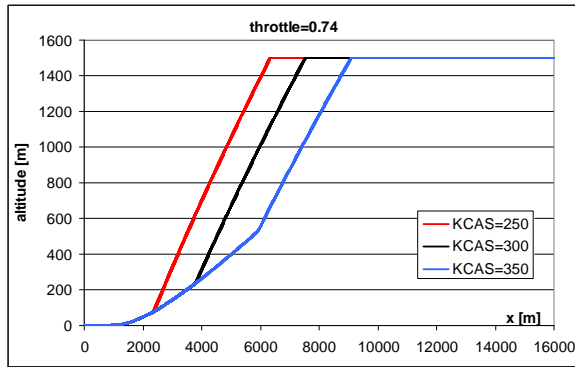


Figure 13: Aircraft take-off trajectories for an F-16 aircraft with constant throttle setting  $th = 0.74$  (just below military power) and for different KCAS on the 2<sup>nd</sup> climb segment.

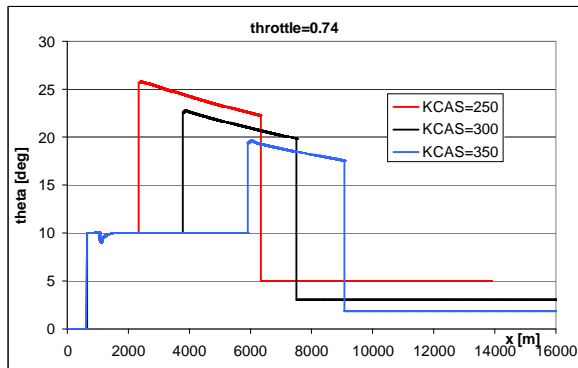


Figure 14: Pitch angle as function of distance  $x$  for take-off's with an F-16 aircraft at constant throttle setting  $th = 0.74$  and for different KCAS on the 2<sup>nd</sup> climb segment.

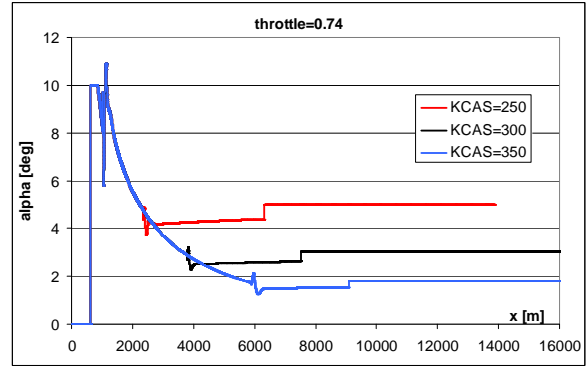


Figure 15: Angle of attack as function of distance  $x$  for take-off's with an F-16 aircraft at constant throttle setting  $th = 0.74$  and for different KCAS on the 2<sup>nd</sup> climb segment.

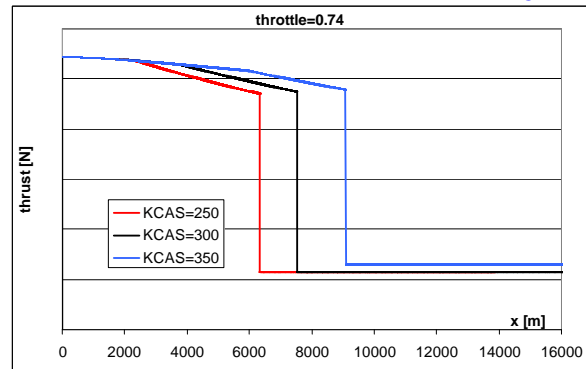
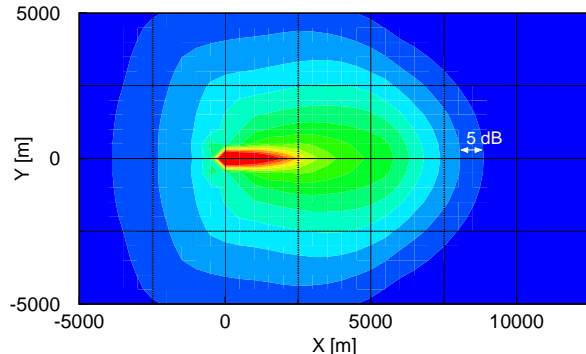
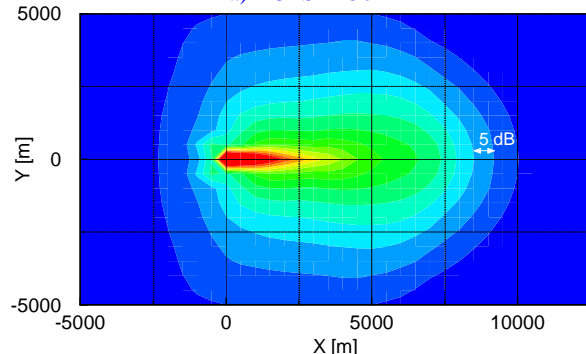


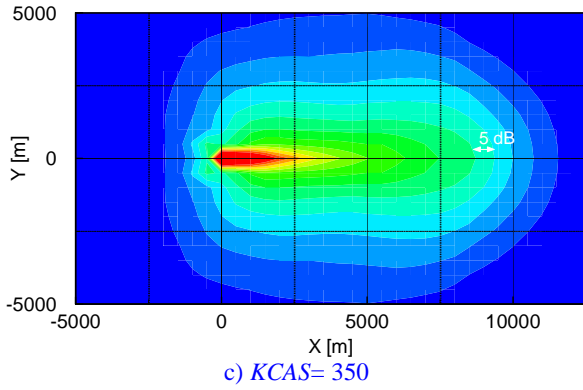
Figure 16: Thrust as function of  $x$  for take-off's with an F-16 aircraft at constant throttle setting  $th = 0.74$  and for different KCAS on the 2<sup>nd</sup> climb segment.



a) KCAS= 250



b) KCAS= 300



c) KCAS= 350

Figure 17:  $L_{A,max}$  contours for take-off's with an F-16 aircraft at constant throttle setting  $th=0.74$  and different KCAS on the 2<sup>nd</sup> climb segment.

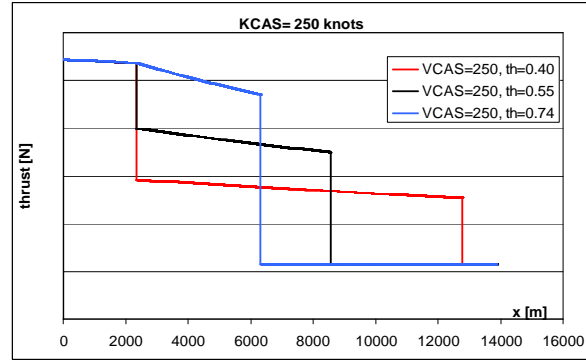


Figure 20: Thrust as function of  $x$  for take-off's with an F-16 aircraft with throttle setting  $th=0.74$  on the 1<sup>st</sup> and KCAS= 250 with various throttle settings on the 2<sup>nd</sup> climb segment.

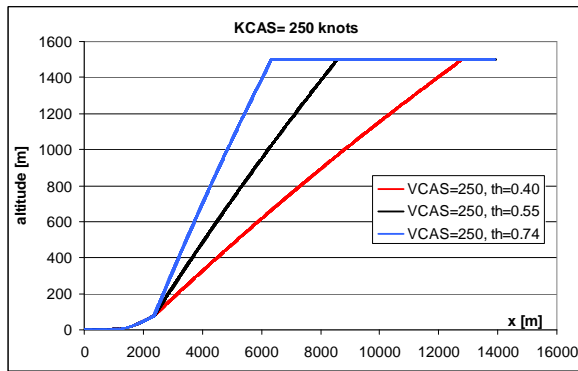


Figure 18: Aircraft take-off trajectories for an F-16 aircraft with throttle setting  $th=0.74$  on the 1<sup>st</sup> and KCAS = 250 with various throttle settings on 2<sup>nd</sup> climb segment.

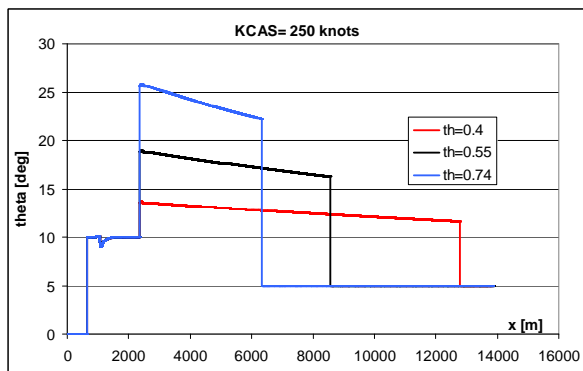
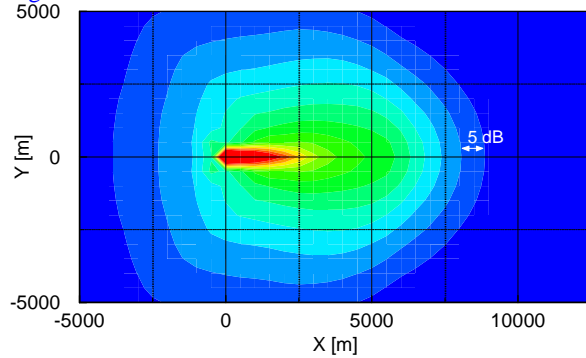
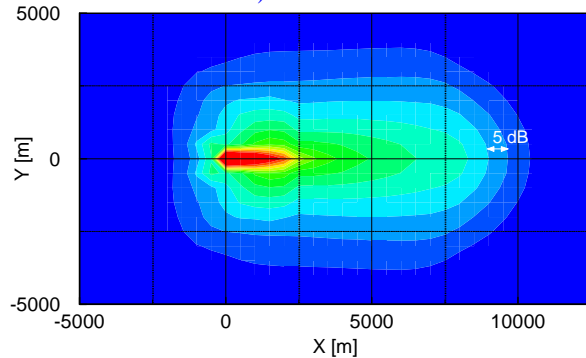


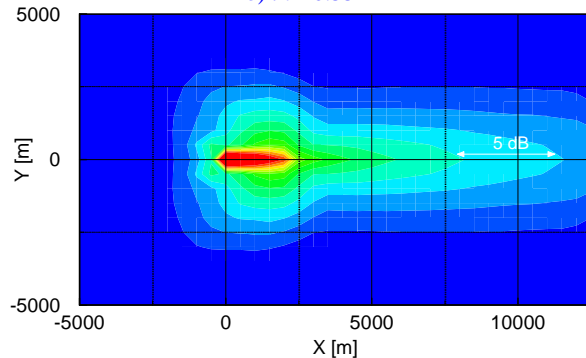
Figure 19: Pitch angle as function of  $x$  for take-off's for an F-16 aircraft with throttle setting  $th=0.74$  on the 1<sup>st</sup> and KCAS= 250 and various throttle settings on the 2<sup>nd</sup> climb segment.



a)  $th=0.74$



b)  $th=0.55$



c)  $th=0.40$

Figure 21:  $L_{A,max}$  contours for take-off's with an F-16 aircraft with throttle setting  $th=0.74$  on the 1<sup>st</sup> and KCAS= 250 with various throttle settings and on the 2<sup>nd</sup> climb segment.

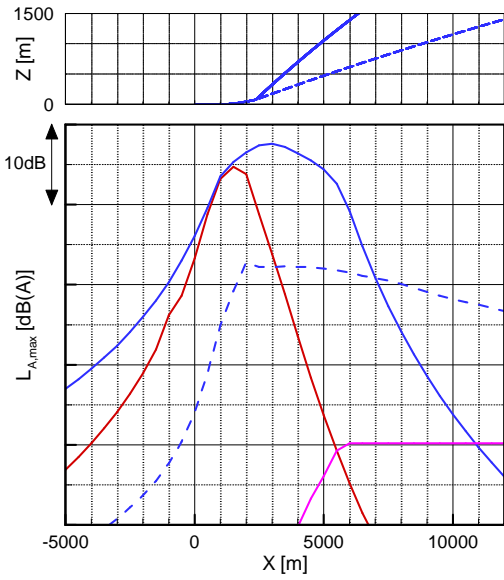


Figure 22: Take-off trajectories (top figure) and  $L_{A,max}$  as function of  $x$  at  $y=1000$  m,  $KCAS=250$  on 2<sup>nd</sup> climb segment. Case without power cutback shows contribution of different flight segments separately: blue solid line for complete climb until reaching final altitude, red line for ground acceleration and initial climb phase only, magenta line for level flight segment. The blue broken line shows contribution of the 2<sup>nd</sup> climb phase for the  $th=0.4$  case.

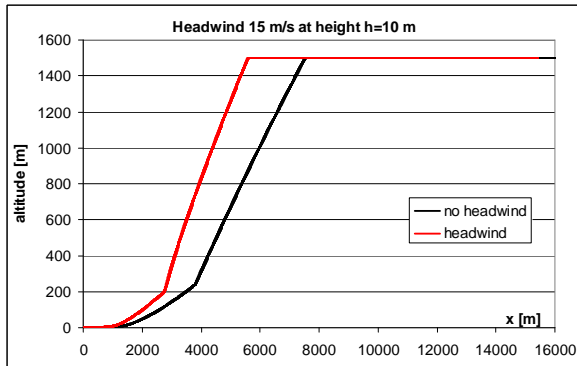
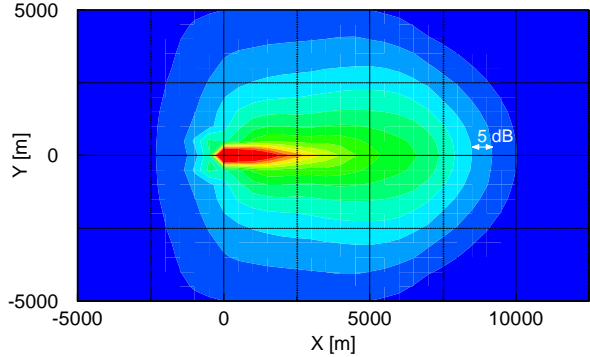
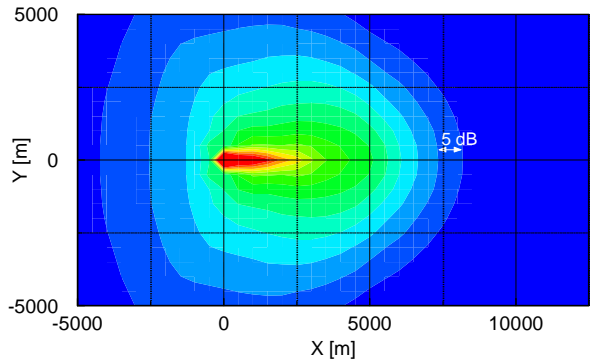


Figure 23: Take-off trajectories for an F-16 aircraft with and without headwind ( $V_{H,10}=15$  m/s,  $V_H=V_{H,10}(h/10)^{0.14}$ ,  $th=0.74$  and  $KCAS=300$  on 2<sup>nd</sup> climb segment.



a) no wind



b) with headwind

Figure 24: Comparison of  $L_{A,max}$  noise footprints for take-off's with an F-16 aircraft, without and with strong headwind ( $V_{H,10}=15$  m/s,  $V_H=V_{H,10}(h/10)^{0.14}$ ,  $th=0.74$  and  $KCAS=300$  on the 2<sup>nd</sup> climb segment.